Volume 2
Number 24
21 December 2021
Pages 7791–7968

Materials Advances

rsc.li/materials-advances

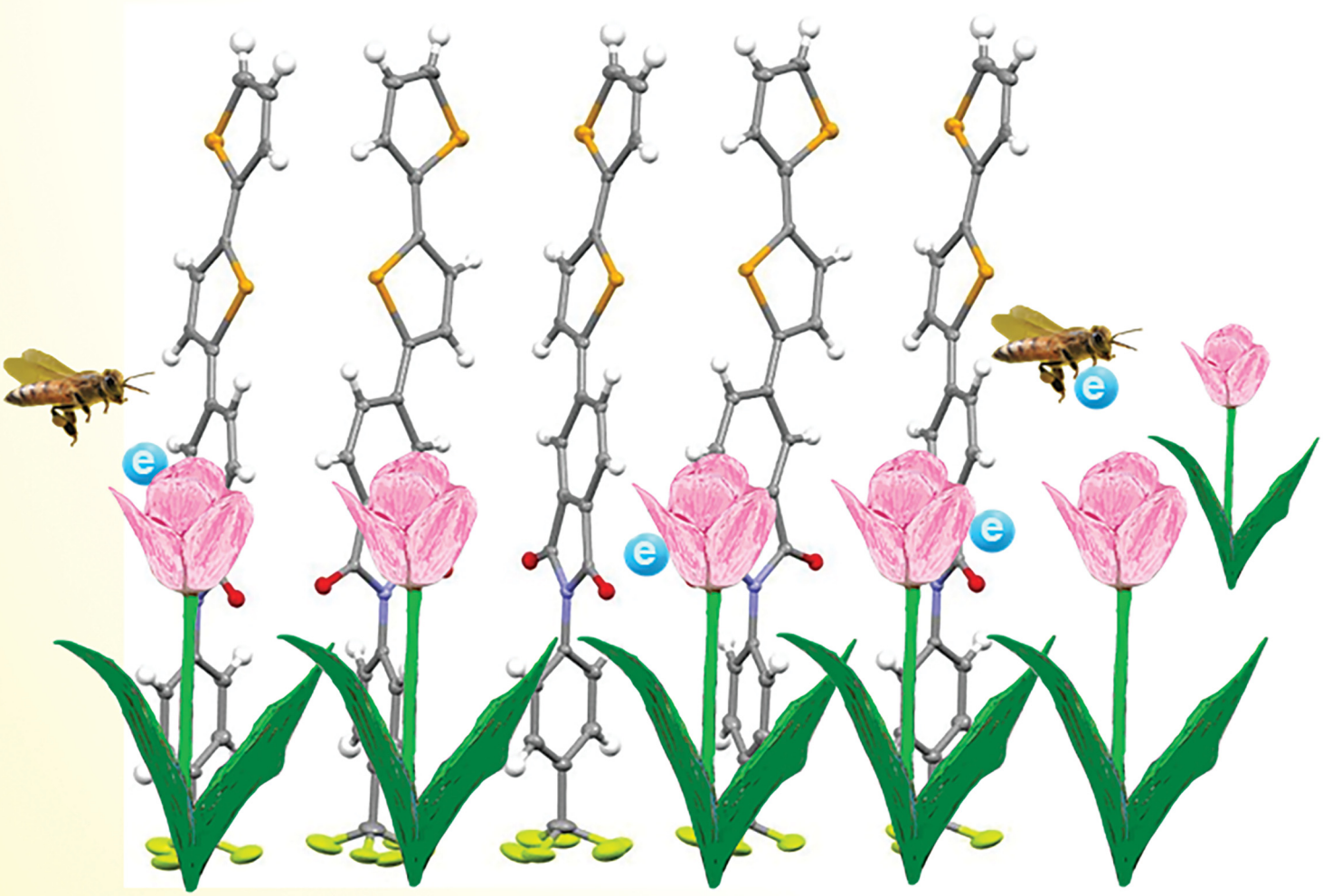

ISSN 2633-5409

ROYAL SOCIETY OF CHEMISTRY

PAPER
Jun-ichi Nishida *et al.*
Synthesis and electron-transport properties of *N*-trifluoromethylphenyl-phthalimides containing selenophene substituents

Materials Advances

ROYAL SOCIETY OF CHEMISTRY

PAPER

View Article Online
View Journal | View Issue

Cite this: *Mater. Adv.*, 2021, 2, 7861

Synthesis and electron-transport properties of *N*-trifluoromethylphenyl-phthalimides containing selenophene substituents†

Jun-ichi Nishida, ‡*[a] Yoshiki Morikawa,‡[a] Akito Hashimoto,‡[a] Yasuyuki Kita,‡[a] Hiroshi Nishimoto,‡[a] Tomofumi Kadoya, ‡[b] Hiroyasu Sato‡[c] and Takeshi Kawase‡[a]

Trifluoromethylphenyl substituted phthalimides (PIs) containing oligoselenophene and phenylselenophene substituents were synthesized. Spectroscopic studies show that increasing the number of selenophene units causes the UV-Vis and photoluminescence maxima of the selenophene substituted PIs to shift to longer wavelengths. Analysis of the single crystal structure shows that the biselenophene substituted derivative has a layered structure, no center of symmetry and a molecular network with close contacts between Se atoms. XRD patterns of the PI derivatives indicate they have similar layered structures. These substances were used to fabricate field-effect transistors (FET)s by using the vapor deposition method. The FET derived using the biselenophene substituted PI exhibits clear n-type characteristics with an electron mobility of *ca.* 10^{-4} cm^2 V^{-1} s^{-1}. The FET prepared using the more highly conjugated terselenophene derivative also displays n-type FET characteristics with a slightly higher threshold voltage. Moreover, n-type behavior is also displayed by a highly crystalline thin film generated from the phenylselenophene derivative. The LED light responsiveness of FET characteristics was investigated. While the FET formed from the terselenophene derivative maintains a saturation drain–source current (I_{DS}) operation along with a three-fold increase of electron mobility upon irradiation, those derived from the biselenophene and phenylselenophene derivatives display Ohm's law-like I_{DS}. The difference in light responses are discussed in terms of conductivity differences.

Received 12th August 2021,
Accepted 27th October 2021

DOI: 10.1039/d1ma00716e

rsc.li/materials-advances

Introduction

Organic n-type semiconductors have attracted great attention because they can be used in various electronic devices such as field-effect transistors (FETs)[1–9] and organic photo-voltaic cells.[10–12] As a result, studies of organic compounds that possess high electron mobilities have received great interest. In addition to these efforts, studies aimed at developing new types of substances with n-type semiconductor features have also focused on creating functional devices and understanding relationships that exist between molecular structures and electron-transport. In the context of FETs, it is known that imide derivatives containing extensive π-conjugated networks exhibit excellent electron mobilities.[13–17] Attempts have also been made to create substances that have n-type semiconductor properties using small imide derivatives such as pyromellitic diimides.[18] These efforts have demonstrated that, in general, good electron transportability exists in substances that possess two phthalimide (PI) moieties and an appropriate conjugated system such as those in anthracenes, pentalenes and pyrenes.[19–21]

The PI moiety is an important electron-acceptor and, as a result, it has been incorporated into electron-acceptor units in electronics.[22–24] An example exists in which microwire crystals of PI derivatives containing a dicyanocorannulene has been used in n-type FETs.[24] However, simple asymmetric PI derivatives linked to several aromatic oligomers have not been usable as n-type semiconductors in FETs.

We anticipated that the electron transport properties of PIs could be enhanced by introducing electron movement pathways, such as networks containing carbonyl units[25] and a 4-trifluoromethylphenyl (CF_3ph) terminal group, and that these systems would be suitable for n-type semiconductors[26] (Fig. 1a). In addition to searching for substances of this type, efforts in

[a] *Department of Applied Chemistry, Graduate School of Engineering, University of Hyogo, Himeji, Hyogo 671-2280, Japan. E-mail: jnishida@eng.u-hyogo.ac.jp*
[b] *Department of Material Science, Graduate School of Science, University of Hyogo, Kouto, Kamigori-cho, Ako-gun, Hyogo 678-1297, Japan*
[c] *Rigaku Corporation, Matsubaracho, Akishima, Tokyo 196-8666, Japan*

† Electronic supplementary information (ESI) available. CCDC 2101621. For ESI and crystallographic data in CIF or other electronic format see DOI: 10.1039/d1ma00716e

‡ Contributed equally to this work.

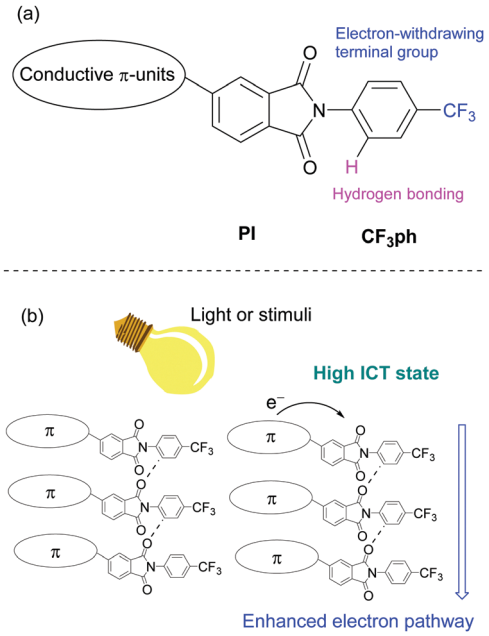

Fig. 1 (a) Molecular design of asymmetric PI compound and (b) the expected electron transporting pathway enhanced by external stimuli.

this area are motivated by the possibility of introducing responsiveness to external stimuli (Fig. 1b). For example, new compounds whose electron mobilities are depending on intramolecular charge transfer (ICT) states by light irradiation may be important components of multi-functional electronic devices[27] and organic photodetectors.[28,29]

In a previous report, we described studies that show that crystals of *N*-CF_3ph-substituted PIs have well-aligned layered structures with no center of symmetry.[30–32] The hydrogen bonding network between PI moieties and CF_3ph groups serves as a template for making these crystals triboluminescent (TL)[30,31] and for increasing excited state lifetimes.[32] A potentially important characteristic of these PI derivatives is that linked conjugated components can be introduced.

The aim of the current investigation was to investigate the physical properties of PI derivatives that contain conductive π-moieties. For this purpose, we prepared the oligoselenophene linked PIs **1–3** and phenylselenophene analogue **4** (Fig. 2). We believed that these substances would have the following advantageous electronic features. Firstly, the large selenium (Se) atom in **1–4** is expected to enhance intermolecular interactions and orbital overlap. In fact, compounds containing selenophene moieties have been shown to have high charge mobilities.[33–36] Secondly, because selenophenes have good electron-donating properties, PI derivatives containing these moieties should possess donor–acceptor (D-A) type structures and display ICT properties.[37–41] Finally, crystals of the *N*-CF_3ph-substituted PIs should have electron-withdrawing layered structures, which enhance the expression of n-type semiconductor characteristics needed for functioning FETs.

In the study described below, we synthesized PI derivatives **1–4**, and carried out an X-ray crystal structure analysis, and

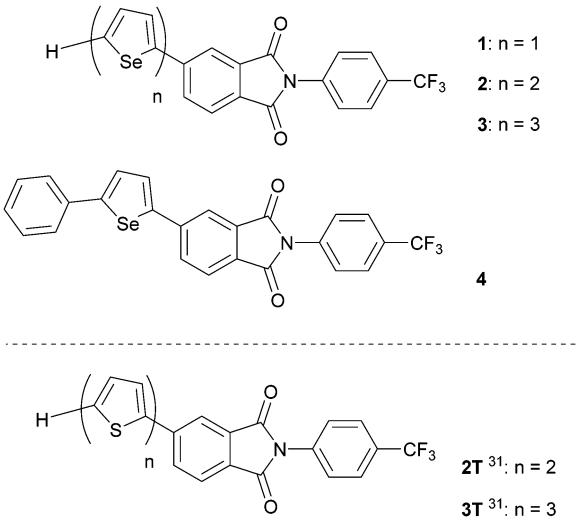

Fig. 2 Molecular structures of PIs **1–4** with selenophene units. Previously reported thiophene derivatives **2T** and **3T**.[31]

spectroscopic and FET characteristics. In the effort, we observed that vapor deposited films of **2–4** function as n-type semiconductors in FETs. In addition, the drain–source currents (I_{DS}) of these FETs irradiated using a light emitting diode (LED) can be controllably enhanced by varying the current flowing through the LED. The results are discussed and compared with those arising from the previously report about thiophene derivatives **2T** and **3T**.[31]

Results and discussion

PIs **2–4** were prepared using the mono-selenophene substituted derivative **1** as the starting material. Synthesis of **1** was accomplished by using Stille coupling reaction of bromo-PI **5** with 2-(tributylstannyl)selenophene (Scheme 1). Bromination of **1** with *N*-bromosuccinimide (NBS) gave bromo-selenophene **6** in 93% yield. Stille coupling reactions of **6** with the corresponding

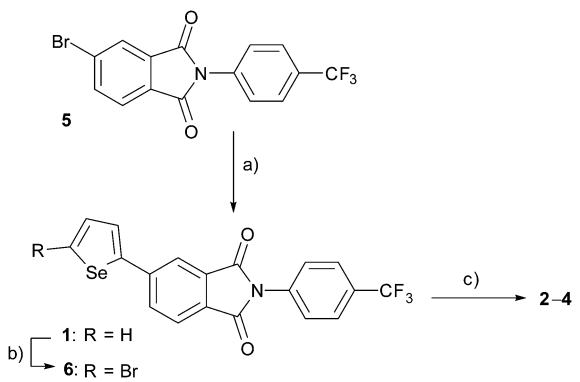

Scheme 1 Preparation of target PIs **1–4** and bromine substituted precursor **6**. Reagents: (a) $Pd(PPh_3)_4$, 2-(tributylstannyl)selenophene (y. 80%), (b) NBS (93%), (c) $Pd(PPh_3)_4$, 2-(tributylstannyl)selenophene for **2** (60%); 5-tributylstannyl-2,2′-biselenophene for **3** (45%); tributylstannylbenzene for **4** (63%).

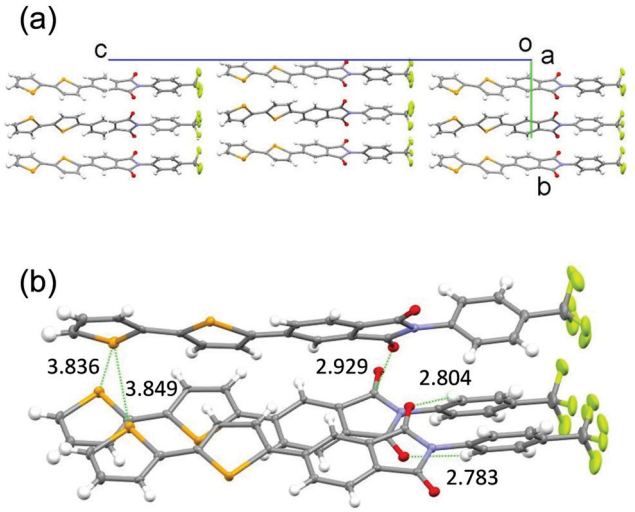

Fig. 3 Crystal packing structures of biselenophene derivative **2**. (a) Viewed along *a*-axis. (b) Close interactions.

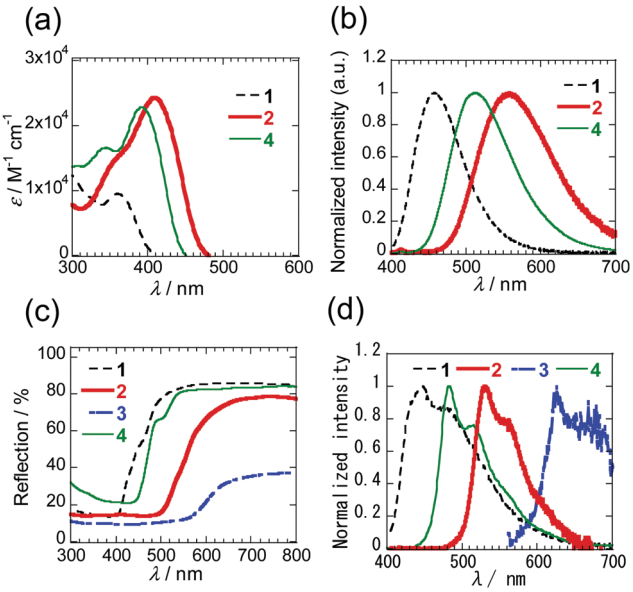

Fig. 4 (a) UV-Vis ($<10^{-5}$ M) and (b) PL spectra of **1**, **2** and **4** in DCM. The spectra of **3** with low solubility are shown in Fig. S3 and S4 (ESI†). (c) Solid diffuse reflection spectra of **1–4**. (d) PL spectra of **1–4** in solid states.

tin reagents then generated the biselenophene, terselenophene and phenylselenophene derivatives **2–4** in 60, 45, and 63% respective yields, which were purified by using recrystallisation from DMF or sublimation.

X-Ray crystal structural analysis was performed (Fig. 3 and Fig. S1A in ESI†)§ on a single crystal of the biselenophene **2**, obtained by recrystallisation from DMF. In the crystal (space group is *Pn*), **2** exists in a well-aligned layered structure with no center of symmetry. Typical hydrogen bonding networks with distances of 2.783 and 2.804 Å exist in the PI and CF_3ph layer between oxygen atoms of carbonyl groups and benzene ring hydrogens (Fig. 3b). Interactions also exist between the carbonyl groups. Moreover, the selenium atoms in the terminal selenophene rings are in close contact with distances of 3.836 and 3.849 Å that are near the sum of the van der Waals radius plus 0.1 Å. The crystal is isomorphic to that of previously reported bithiophene substituted PI **2T**. However, the fact that the distances between the sulfur (S) atoms of the terminal thiophene rings in **2T** (3.860 and 3.863 Å) are almost the same as those between the Se atoms in **2** suggests that intermolecular interaction between the Se atoms in **2** is larger than that between the S atoms in **2T**.

The respective PIs **1–4** are colourless, orange, dark red and yellow in solution and the solid states. Inspection of the absorption spectra of **1–4** in dichloromethane (DCM) (Fig. 4a and Fig. S3, ESI†) shows that the mono-selenophene derivative **1** has a maximum at 360 nm, and that **2** and **3** containing more extensively conjugated biselenophenes have respective maxima at 411 and 436 nm. The absorption maximum of biselenophene **2** occurs at a longer wavelength than that of the bithiophene **2T** (399 nm). Moreover, elongation of the conjugated system by incorporation of phenyl group in **4** leads to a small increase in the wavelength maximum. Analysis of the photoluminescence (PL) spectra of these substances in DCM shows that the emission maximum is shifted to longer wavelengths when the number of selenophene rings increases (Fig. 4b). The same trends are observed for maxima in PL spectra of solid states of these substances (Fig. 4d). Solid diffuse reflection spectra of these PIs are given in Fig. 4c and Fig. S5 (ESI†). The peak-onset of **1** takes place at *ca.* 520 nm. As the number of selenophene rings increases, the peak-onset shifts to longer wavelengths (650 nm for **2** and 660 nm for **3**). The spectroscopic data for these PI derivatives is given in Table 1.

In addition, to evaluate the properties of PIs **2** and **3** in the thin films, absorption spectra were measured on thin films (60 nm) vacuum-deposited on quartz glasses (Fig. S6, ESI†). The longest absorption peaks occur at the shorter wavelengths (400 nm for **2** and 376 nm for **3**) than those in DCM. Shifts to longer wavelengths are observed at the absorption ends, which are the result of aggregation.

Table 1 Optical and electrochemical data of **1–4**

Compd	λ_{abs} [a] (nm) (log ε)	λ_{em} [ab] (nm) (Φ)	$\lambda_{end\text{-}abs\_solid}$ [c] (nm)	λ_{em_solid} [d] (nm) (Φ)	E_{red} [e]
1	360 (3.98)	458 (0.16)	520	448 (—)[g]	−1.68
2	411 (4.39)	555 (0.04)	650	531 (0.05)	−1.64
3	436 (—)[f]	587 (—)[g]	660	625 (—)[g]	—[f]
4	392 (4.36)	515 (0.13)	540	483 (0.10)	−1.63

[a] In CH_2Cl_2. [b] Estimated by using 9,10-diphenylanthracene (λ_{ex} = 366 nm, Φ = 0.86 in cyclohexane) as a standard.[42] [c] Estimated from tangent intersections in solid diffuse reflection spectra. [d] Integrating sphere (λ_{ex} = 366 nm). [e] *V vs.* Fc/Fc$^+$, 0.1 M *n*-Bu_4NPF_6 in DMF, Pt electrode. Scan rate 100 mV s^{-1}. [f] Low solubility. [g] Too low to decide.

§ Crystal data for **2**: an orange plate crystal, $C_{23}H_{12}F_3NO_2Se_2$, M = 549.26, crystal dimensions 0.077 × 0.034 × 0.008 mm, monoclinic, space group *Pn*, a = 5.77820(14), b = 7.8504(2), c = 42.3511(12) Å, β = 91.026(3), V = 1920.80(9) Å^3, Z = 4, D_c = 1.899 g cm^{-3}, 23 086 reflections collected, 6272 independent (R_{int} = 0.0320), GOF = 1.051, R_1 [$F^2 > 2\sigma(F^2)$] = 0.0339, and w$R2(F^2)$ = 0.0921 for all reflections. Flack parameter 0.019(14). CCDC number is 2101621.

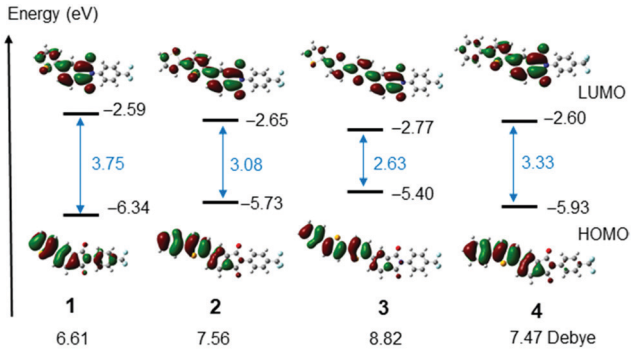

Fig. 5 HOMOs and LUMOs of PIs **1–4** calculated using Gaussian 09 at RB3LYP/6-31G(d,p) level of theory. Dipole moments were also added.

To gain an understanding of the electronic transitions of the selenophene substituted PIs, calculations were performed at the RB3LYP/6-31G(d,p) level.[43] The HOMOs and LUMOs of PIs **1–4** are shown in Fig. 5 and Fig. S17 (ESI†). The HOMO energy of mono-selenophene derivative **1** is 6.34 eV. As the conjugated system is extended to form biselenophene **2** and terselenophene **3**, the energy of the HOMO increases and that of the LUMO decreases, leading to a smaller HOMO–LUMO energy gap. TD-DFT calculations were performed to assess the ICT nature of the electronic transitions. The results show that the oscillator strength is significantly enhanced as the number of selenophene rings in the PI derivatives increases. The data are summarized in Table 2 and calculated dipole moments are shown in Fig. 5.

The redox potentials of the selenophene substituted PIs were determined by using cyclic voltammetry (CV). PIs **1**, **2** and **4** in DMF show cleanly reversible reduction waves (E_{red} of **1**: −1.68, **2**: −1.64, **4**: −1.63 V *vs.* ferrocene (Fc)/Fc^+) (Fig. S8, ESI†). Based on 4.8 eV of the HOMO of ferrocene, the LUMO energy of **2** is 3.2 eV.[44] Compounds having the LUMO energy exhibit n-type semiconductor properties for FET, but tend to have high threshold voltages (V_{th}).[26] On the other hand, in thin film states, electron injection seems to be improved. CV measurements on thin films of **2** and **3** deposited on ITO electrodes immersed in acetonitrile showed that reduction waves rise from around −1.1 V (*ca.* 3.6 eV) (Fig. S9, ESI†).

Bottom-contact type FETs were fabricated by using a vacuum deposition method with substrates equipped with interdigitated Au electrodes.[45] A small white light emitting diode[46] was installed on a shutter used for vapor deposition so that the distance from the substrate is controlled to be 1 cm (Fig. S10, ESI†). Surface treatment reagents such as hexamethyldisilazane were not used to avoid the possible occurrence of electron transfer between these reagents and PI derivatives during photoirradiation.

Measurements of the FETs were carried out at room temperature and under high vacuum conditions (10^{-5} Pa). PI derivatives **2–4** exhibit clear n-type characteristics. First, the FET containing biselenophene derivative **2** in the dark exhibits characteristic output curves with normal saturation current with the electron mobility of 1.3×10^{-4} cm^2 V^{-1} s^{-1} (Fig. 6a).[47] The electron mobility is enhanced to 8.9×10^{-4} cm^2 V^{-1} s^{-1} by raising the substrate temperature to 100 °C during vapor deposition (Fig. S14, ESI†). The film containing the π-extended terselenophene derivative **3** also exhibits n-type FET behavior with a slightly high electron-mobility (4.2×10^{-4} cm^2 V^{-1} s^{-1}) and V_{th} (+29 V). The difference of V_{th} is consistent with the increased electron donating property of the π-extended selenophene group in **3**. The FET containing phenylselenophene substituted PI **4** has a higher electron mobility compared with that of biselenophene **2** made at room temperature substrate. The data are summarized in Table 3.

Next, the effect of light irradiation on the characteristics of FETs prepared using these selenophene containing PI derivatives was assessed. An LED was employed for this purpose and the current flowing through the LED is given as I_{LED}.[46] A large amplification of the drain–source current (I_{DS}) with respect to drain–source voltage (V_{DS}) is observed. In the case of the FET prepared using **2**, the maximum I_{DS} increases approximately six times when I_{LED} is 12.9 mA (Fig. 6d). No saturation I_{DS} is observed, and the values increase in a manner that follows Ohm's law. The electron mobility, calculated by using a plot of $I_{DS}^{1/2}$ (at V_{DS} 100 V) *vs.* V_G,[47] is estimated to be small because the V_G dependence is small (Table 3). The increase of I_{DS} promoted by irradiation is related to an increase in conductivity.[48] An about three hundred times increase (Table 3) in conductivity, calculated as the difference when the gate voltage is not applied, is brought about by irradiation of FET **2**.

On the other hand, in the output of the FET device containing **3** maintains saturation I_{DS} during photoirradiation. The results of similar calculations[47] show that the system has an approximately three times higher mobility and a lower V_{th} of +21 V (Table 3). The I_{DS} response of the FET device made using **4** to photoirradiation is similar to that of **2**, and the relationship between I_{DS} and V_{DS} is in accord with Ohm's law. The differences between the terselenophene derivative **3** and analogues **2** and **4** is likely the result of the differing lengths of their conjugated systems linked to the PI core.

In this system, ICT in conjugated systems containing PI core caused by light irradiation work to reduce V_{th} of electron transport. A long conjugated system gives a large V_{th}, but it stabilizes the characteristics of FET. Moreover, it might be possible to stabilize the FET characteristics even under photoirradiation by increasing the length of the systems. The increase in the rate of change in the maximum I_{DS} is about 4 times large but the low off-current is maintained.

Table 2 Selected absorption peaks of **1–4** calculated by using the TD-DFT method[a]

	Absorption/nm (Oscillator strength: *f*)	Assignments (ratios of contribution)
1	381 (0.152)	HOMO to LUMO (66%)
2	446 (0.564)	HOMO to LUMO (70%)
3	517 (0.998)	HOMO to LUMO (70%)
4	418 (0.470)	HOMO to LUMO (69%)

[a] Calculated at the RB3LYP/6-31G(d,p) level of theory.

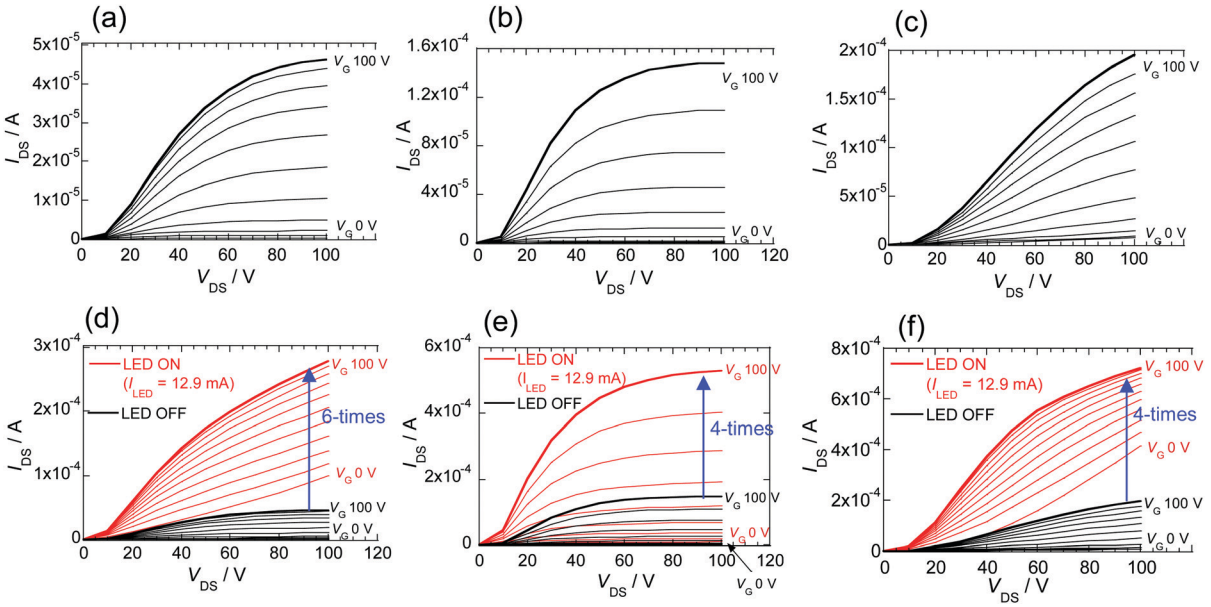

Fig. 6 FET characteristics of (a) biselenophene derivative **2**, (b) terselenophene derivative **3**, and (c) phenylselenophene derivative **4** under dark conditions. FET characteristics of (d) **2**, (e) **3**, and (f) **4** during photoirradiation (bold red lines). Solid black lines are output curves under dark conditions.

Table 3 Electron mobilities,[a] threshold voltages estimated from FET devices, and approximate electrical conductivity[b] of **2–4** and **3T** with and without photoirradiation

Compd and condition	Mobilities ($cm^2\ V^{-1}\ s^{-1}$)	Threshold voltage (V)	Conductivity at V_G = 0 V ($S\ m^{-1}$)
2 (in dark)	1.3×10^{-4}	5	4.6×10^{-6}
2 (in LED)[c]	7.7×10^{-5}	$\ll 0$[e]	1.4×10^{-3}
2 (in dark)[d]	8.9×10^{-4}	<0	1.1×10^{-4}
2 (in LED)[d]	6.6×10^{-4}	$\ll 0$[e]	9.7×10^{-3}
3 (in dark)	4.2×10^{-4}	29	2.0×10^{-7}
3 (in LED)	1.2×10^{-3}	21	3.8×10^{-5}
4 (in dark)	5.9×10^{-4}	<0	1.7×10^{-4}
4 (in LED)	1.0×10^{-4}	$\ll 0$[e]	7.6×10^{-3}
3T (in dark)	2.9×10^{-5}	35	7.7×10^{-8}
3T (in LED)	1.2×10^{-4}	23	3.1×10^{-6}

[a] Calculated from slopes of root I_{DS} ($I_{DS}^{1/2}$) *vs.* V_G. [b] Calculated from slope of I_{DS} *vs.* V_{DS} (between 0 and 100 V). [c] I_{LED} = 12.9 mA. FETs of other compounds were performed in almost similar photoirradiation conditions. [d] Film deposited at substrate temp. 100 °C. [e] Large negative values.

FETs generated using the related thiophene derivatives **2T** and **3T** were also subjected to measurements under the same conditions. A thin film containing the bithiophene **2T** does not display FET characteristics, while that made from **3T** displays n-type character (Fig. S12A, ESI†). While the electron mobility of the FET from **3T** is almost an order of magnitude lower than that of the FET containing terselenophene **3**, its responsiveness to light is close to that of **3**. The results of these experiments suggest that photoirradiation of the FETs produces carriers required for electron transport on the thin film surface, and that the degree of change promoted by light depends on the molecular structure of the substituent on the PI backbone.

The relationship between the intensity of light of LED and amplification of the I_{DS} for the FET devices was explored. The light intensity was adjusted by varying the I_{LED} of the LED source (0.01, 0.28, 1.00, 1.75, 4.86, 7.72, 12.9 mA) (Fig. S11B). In the case of the FET composed of **2**, I_{DS}–V_{DS} curves at V_G = 0 V were extracted from measurements under each photoirradiation condition (Fig. S15, ESI†). Inspection of the results (Fig. 7a) shows that the I_{DS} values and slopes of the I_{DS}–V_{DS} plot increase as I_{LED} values increase. Furthermore, the plot given in Fig. 7b shows that maximum values of I_{DS} (at V_G = 0, and V_{DS} = 100 V), which depend on the I_{LED} values, change significantly at the initial stage when I_{LED} is small and reach a maximum value as the light intensity increases. Overall, the observations shows that the substances in the thin films are sensitive to light and that the I_{DS} values can be controlled by varying the intensity of light. In this way, the LED can act as another gate for transistors of this type. In Fig. 7c is shown a graph of the continuous changes occurring I_{DS} as the LED is repeatedly switched on and off. Results of experiments when the V_G of 100 V is applied are given in Fig. 7d–f. Synergistic use of V_G and light is also possible.

To determine the relationship that exists between molecular structures of the PI derivatives and FET characteristics, X-ray diffraction (XRD) patterns (a reflection mode) were obtained on the solid powders of **2–4** (Fig. 8a–c). Sharp reflection peaks are observed with the first reflection peaks corresponding to *d*-spacings of 21.3, 24.8 and 21.7 Å, which correspond to molecular lengths. The *d*-spacing value was also obtained for the mono-selenophene substituted **1** (Fig. S7A, ESI†). The results suggest that layered structures matching the molecular lengths are formed in the solid states. Next, XRD patterns of deposited films were obtained (Fig. 8d–f). High-order diffraction peaks are observed in the films of **2** and **4**, with corresponding *d*-values from the first reflection peaks of 21.0 and 21.1 Å, which approximately match those in the solid states of these substances.

A weak layered structure seems to exist in the thin film of **3**. The result suggests that the presence of a long π-conjugated

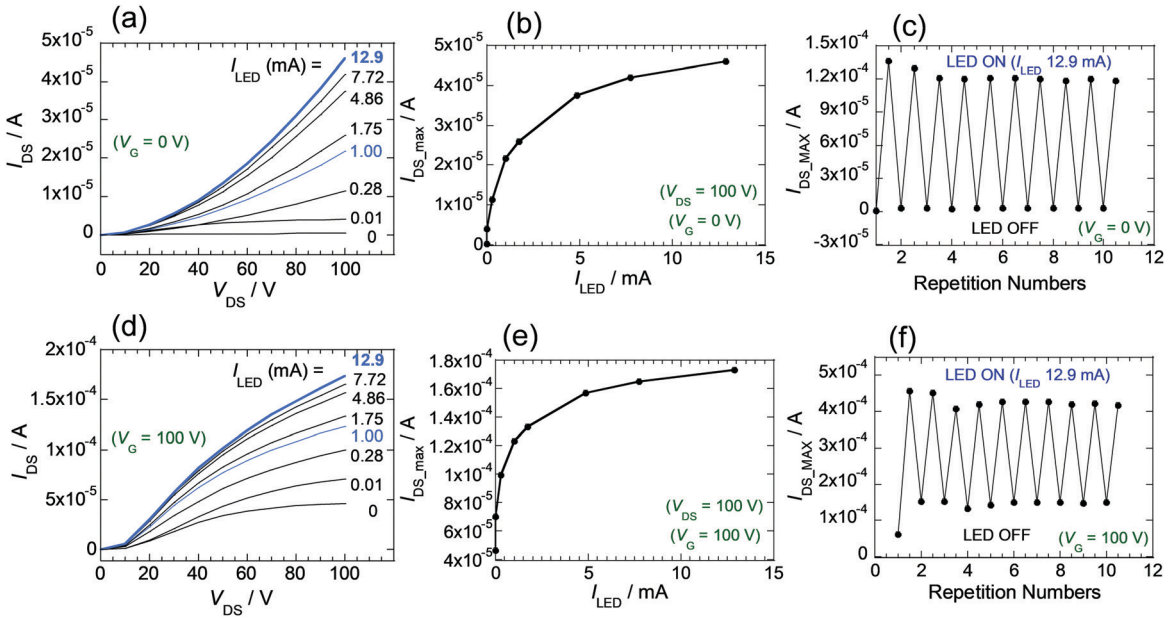

Fig. 7 (a) I_{DS} plots for FET **2** depending on I_{LED} (at V_G = 0 V). (b) I_{DS} maxima of FET **2** with respect to I_{LED}, (at V_G = 0 V, and V_{DS} = 100 V). (c) Changes in I_{DS} values of FET **2** at V_G = 0 V, when LED is switched on and off, repeatedly. (d–f) Similar experimental plots performed at V_G 100 V.

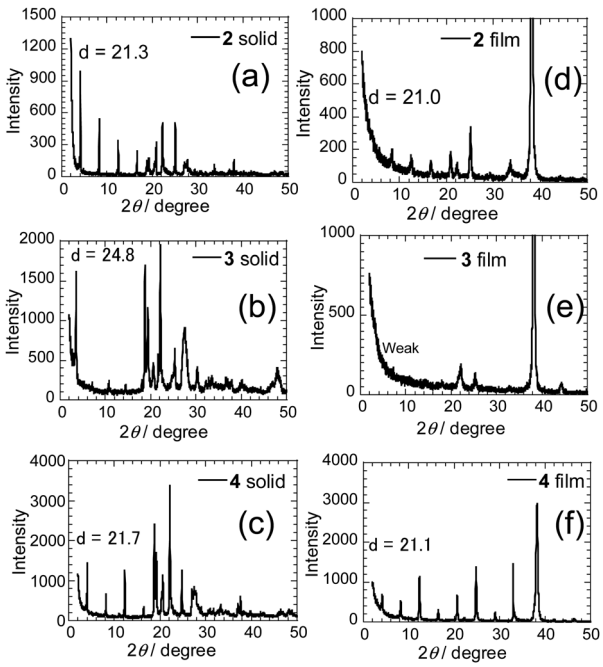

Fig. 8 XRD patterns of powders of (a) **2**, (b) **3** and (c) **4**, and thin films of (d) **2**, (e) **3** and (f) **4**.

substituent on the PI unit may lead to disadvantageous formation of a regular vapor deposition film. Moreover, high-order diffraction peaks were not observed in XRD patterns of films of thiophene-substituted PIs **2T** and **3T**. Thus, intermolecular interactions might be weaker in the thiophene derivatives than they are in the corresponding selenophene derivatives. On the other hand, the terminal phenylselenophene substituted analogue **4** shows strong diffraction peaks in both the solid state and thin film (Fig. 8c and f). Although the origin is unclear, thin films with high diffraction intensities tend to give larger current values and lower V_{th}.

In order to estimate the degree of the intermolecular interaction present in **2**, the overlap integral was calculated using crystal structure data and the Energy Band Calculation program[49] and compared with that reported for the bithiophene derivative **2T**. The results show that a rather large degree of overlap up to 2.5×10^{-3} exists in the LUMO of **2** (Fig. 9) with relatively large values in the directions of t5 and t6. The overlap

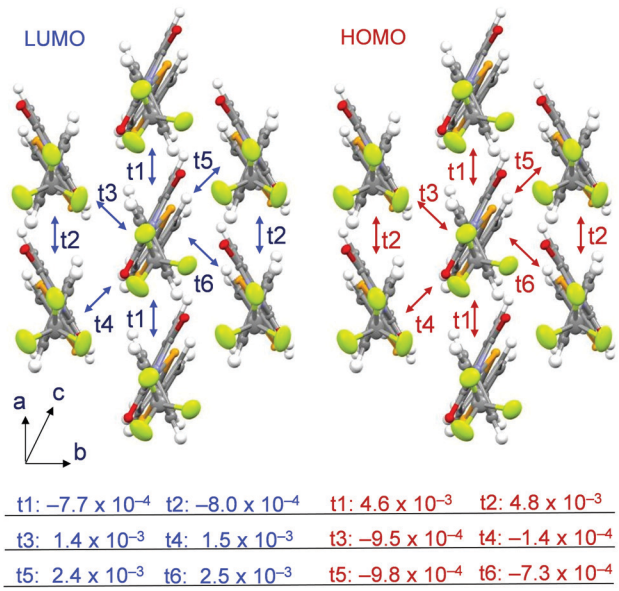

Fig. 9 HOMO and LUMO overlap integrals of **2** estimated by using the energy band calculation program.

is similar to that in the LUMO of bithiophene **2T** (Fig. S18, ESI†). On the other hand, a clear difference exists in the degree of overlap of the HOMOs. In the selenophene derivative **2**, a maximum HOMO overlap value of 4.8×10^{-3} exists in the t2 direction, while it is 6.3×10^{-4} in the thiophene derivative **2T**. The difference, which is likely a consequence of the larger atomic size of Se, is one reason for the different behaviors of vapor-deposited films of **2** and **2T**.

Conclusions

In the study described above, we synthesized CF_3ph-substituted asymmetric PI derivatives containing oligoselenophene and phenylselenophene substituents, and examined their optical and semiconductor properties. We found that derivatives containing the biselenophene or more highly conjugated unit, function as n-type semiconductors in FETs. Moreover, films on which these substances are deposited display a significant increase in I_{DS} values and large shifts in V_{th} in response to visible light. This finding suggests that the controllable effect of light on the transistor properties of these FETs might be useful as a gate or when combined with a gate voltage.

The results arising from these efforts do not enable us to discuss relationships that might exist between solid state photoresponsiveness and the presence or absence of a center of symmetry in the crystalline molecular arrangements. In any event, the selenophene substituted PIs probed in the study are expected to serve as model compounds to more carefully investigate the issue.

Conflicts of interest

There are no conflicts to declare.

Acknowledgements

This study was financially supported by a Grant-in-Aid for Scientific Research on Innovation Areas "Stimuli-responsive Chemical Species for the Creation of Functional Molecules" (No. 2408) (JSPS KAKENHI Grant Number JP15H00959), and Scientific Research C (No. JP16K05896), (JP20K05651), (JP18K05091), (JP21K05024) and (JP20K15356). We thanks to the Division of Instrumental Analysis, Okayama University Advanced Science Research Center, for elemental analyses. We also thanks to Mr Tomoko Amimoto, the Natural Science Center for Basic Research and Development (N-BARD), Hiroshima University, for the HR-EI-MS measurements.

Notes and references

1 C. R. Newman, C. D. Frisbie, D. A. da Silva Filho, J. L. Bredas, P. C. Ewbank and K. R. Mann, *Chem. Mater.*, 2004, **16**, 4436–4451.
2 A. R. Murphy and J. M. J. Frechet, *Chem. Rev.*, 2007, **108**, 1066–1096.
3 Y. Sun, Y. Liu and D. Zhu, *J. Mater. Chem.*, 2005, **15**, 53–65.
4 A. Facchetti, Y. Deng, A. Wang, Y. Koide, H. Sirringhaus, T. J. Marks and R. H. Friend, *Angew. Chem., Int. Ed.*, 2000, **39**, 4547–4551.
5 H. Usta, C. Risko, Z. Wang, H. Huang, M. K. Deliomeroglu, A. Zhukhovitskiy, A. Facchetti and T. J. Marks, *J. Am. Chem. Soc.*, 2009, **131**, 5586–5608.
6 Z. Liang, Q. Tang, J. Xu and Q. Miao, *Adv. Mater.*, 2011, **23**, 1535–1539.
7 P. R. L. Malenfant, C. D. Dimitrakopoulos, J. D. Gelorme, L. L. Kosbar, T. O. Graham, A. Curioni and W. Andreoni, *Appl. Phys. Lett.*, 2002, **80**, 2517–2519.
8 B. J. Jung, N. J. Tremblay, M.-L. Yeh and H. E. Katz, *Chem. Mater.*, 2011, **23**, 568–582.
9 H. Li, F. S. Kim, G. Ren and S. A. Jenekhe, *J. Am. Chem. Soc.*, 2013, **135**, 14920–14923.
10 S. Jinnai, Y. Ie, Y. Kashimoto, H. Yoshida, M. Karakawa and Y. Aso, *J. Mater. Chem. A*, 2017, **5**, 3932–3938.
11 H. Li, T. Earmme, G. Ren, A. Saeki, S. Yoshikawa, N. M. Murari, S. Subramaniyan, M. J. Crane, S. Seki and S. A. Jenekhe, *J. Am. Chem. Soc.*, 2014, **136**, 14589–14597.
12 M. Du, Y. Chen, J. Li, Y. Geng, H. Ji, G. Li, A. Tang, Q. Guo and E. Zhou, *J. Phys. Chem. C*, 2020, **124**, 230–236.
13 A. S. Molinari, H. Alves, Z. Chen, A. Facchetti and A. F. Morpurgo, *J. Am. Chem. Soc.*, 2009, **131**, 2462–2463.
14 T. Okamoto, S. Kumagai, E. Fukuzaki, H. Ishii, G. Watanabe, N. Niitsu, T. Annaka, M. Yamagishi, Y. Tani, H. Sugiura, T. Watanabe, S. Watanabe and J. Takeya, *Sci. Adv.*, 2020, **6**, eaaz0632.
15 K. Tajima, K. Matsuo, H. Yamada, S. Seki, N. Fukui and H. Shinokubo, *Angew. Chem., Int. Ed.*, 2021, **60**, 14060–14067.
16 A. N. Lakshminarayana, A. Ong and C. Chi, *J. Mater. Chem. C*, 2018, **6**, 3551–3563.
17 J. T. T. Quinn, J. Zhu, X. Li, J. Wang and Y. Li, *J. Mater. Chem. C*, 2017, **5**, 8654–8681.
18 Q. D. Zheng, J. Huang, A. Sarjeant and H. E. Katz, *J. Am. Chem. Soc.*, 2008, **130**, 14410–14411.
19 Z. Wang, C. Kim, A. Facchetti and T. J. Marks, *J. Am. Chem. Soc.*, 2007, **129**, 13362–13363; H. Usta, C. Kim, Z. Wang, S. Lu, H. Huang, A. Facchetti and T. J. Marks, *J. Mater. Chem.*, 2012, **22**, 4459–4472.
20 G. Dai, J. Chang, L. Jing and C. Chi, *J. Mater. Chem. C*, 2016, **4**, 8758–8764.
21 Y. Li, Z. Yao, J. Xie, H. Han, G. Yang, X. Bai, J. Pei and D. Zhao, *J. Mater. Chem. C*, 2021, **9**, 7599–7606.
22 H. Bock, D. Subervie, P. Mathey, A. Pradhan, P. Sarkar, P. Dechambenoit, E. A. Hillard and F. Durola, *Org. Lett.*, 2014, **16**, 1546–1549.
23 M. Li, H.-Y. Lu, C. Zhang, L. Shi, Z. Tang and C.-F. Chen, *Chem. Commun.*, 2016, **52**, 9921–9924.
24 R. Chen, R.-Q. Lu, K. Shi, F. Wu, H.-X. Fang, Z.-X. Niu, X.-Y. Yan, M. Luo, X.-C. Wang, C.-Y. Yang, X.-Y. Wang, B. Xu, H. Xia, J. Pei and X.-Y. Cao, *Chem. Commun.*, 2015, **51**, 13768–13771.
25 An example of n-type semiconductor containing a hydrogen bonding network: J.-I. Nishida, T. Fujita, Y. Fujisaki,

S. Tokito and Y. Yamashita, *J. Mater. Chem.*, 2011, **21**, 16442–16447.

26 S. Ando, J.-i. Nishida, E. Fujiwara, H. Tada, Y. Inoue, S. Tokito and Y. Yamashita, *Chem. Mater.*, 2005, **17**, 1261–1264; S. Ando, J.-i. Nishida, H. Tada, Y. Inoue, S. Tokito and Y. Yamashita, *J. Am. Chem. Soc.*, 2005, **127**, 5336–5337.

27 E. Orgiu and P. Samorì, *Adv. Mater.*, 2014, **26**, 1827–1845.

28 B. Zhang, M. T. Trinh, B. Fowler, M. Ball, Q. Xu, F. Ng, M. L. Steigerwald, X.-Y. Zhu, C. Nuckolls and Y. Zhong, *J. Am. Chem. Soc.*, 2016, **138**, 16426–16431.

29 Z. Su, F. Hou, X. Wang, Y. Gao, F. Jin, G. Zhang, Y. Li, L. Zhang, B. Chu and W. Li, *ACS Appl. Mater. Interfaces*, 2015, **7**, 2529–2534.

30 H. Nakayama, J.-i. Nishida, N. Takada, H. Sato and Y. Yamashita, *Chem. Mater.*, 2012, **24**, 671–676.

31 J.-i. Nishida, H. Ohura, Y. Kita, H. Hasegawa, T. Kawase, N. Takada, H. Sato, Y. Sei and Y. Yamashita, *J. Org. Chem.*, 2016, **81**, 433–441.

32 Y. Kita, J.-i. Nishida, S. Nishida, Y. Matsui, H. Ikeda, Y. Hirao and T. Kawase, *ChemPhotoChem*, 2018, **2**, 42–52.

33 Y. Kunugi, K. Takimiya, K. Yamane, K. Yamashita, Y. Aso and T. Otsubo, *Chem. Mater.*, 2003, **15**, 6–7.

34 Y. Kunugi, K. Takimiya, Y. Toyoshima, K. Yamashita, Y. Aso and T. Otsubo, *J. Mater. Chem.*, 2004, **14**, 1367–1369.

35 R. M. Osuna, R. P. Ortiz, T. Okamoto, Y. Suzuki, S. Yamaguchi, V. Hernández and J. T. L. Navarrete, *J. Phys. Chem. B*, 2007, **111**, 7488–7496.

36 P.-O. Schwartz, S. Förtsch, A. Vogt, E. Mena-Osteritz and P. Bäuerle, *Beilstein J. Org. Chem.*, 2019, **15**, 1379–1393.

37 S. S. Zade and M. Bendikos, *Chem. – Eur. J.*, 2008, **14**, 6734–6741.

38 S. Haid, A. Mishra, C. Uhrich, M. Pfeiffer and P. Bäuerle, *Chem. Mater.*, 2011, **23**, 4435–4444.

39 T. Okamoto, K. Kudoh, A. Wakamiya and S. Yamaguchi, *Org. Lett.*, 2005, **7**, 5301–5304.

40 Y.-C. Pao, Y.-L. Chen, Y.-T. Chen, S.-W. Cheng, Y.-Y. Lai, W.-C. Huang and Y.-J. Cheng, *Org. Lett.*, 2014, **16**, 5724–5727.

41 W. Xu, M. Wang, Z. Ma, Z. Shan, C. Li and H. Wang, *J. Org. Chem.*, 2018, **83**, 12154–12163.

42 J. V. Morris, M. A. Mahaney and J. R. Huber, *J. Phys. Chem.*, 1976, **80**, 969–974.

43 M. J. Frisch, G. W. Trucks, H. B. Schlegel, G. E. Scuseria, M. A. Robb, J. R. Cheeseman, G. Scalmani, V. Barone, B. Mennucci, G. A. Petersson, H. Nakatsuji, M. Caricato, X. Li, H. P. Hratchian, A. F. Izmaylov, J. Bloino, G. Zheng, J. L. Sonnenberg, M. Hada, M. Ehara, K. Toyota, R. Fukuda, J. Hasegawa, M. Ishida, T. Nakajima, Y. Honda, O. Kitao, H. Nakai, T. Vreven, J. A. Montgomery Jr., J. E. Peralta, F. Ogliaro, M. J. Bearpark, J. Heyd, E. N. Brothers, K. N. Kudin, V. N. Staroverov, R. Kobayashi, J. Normand, K. Raghavachari, A. P. Rendell, J. C. Burant, S. S. Iyengar, J. Tomasi, M. Cossi, N. Rega, N. J. Millam, M. Klene, J. E. Knox, J. B. Cross, V. Bakken, C. Adamo, J. Jaramillo, R. Gomperts, R. E. Stratmann, O. Yazyev, A. J. Austin, R. Cammi, C. Pomelli, J. W. Ochterski, R. L. Martin, K. Morokuma, V. G. Zakrzewski, G. A. Voth, P. Salvador, J. J. Dannenberg, S. Dapprich, A. D. Daniels, O. Farkas, J. B. Foresman, J. V. Ortiz, J. Cioslowski and D. J. Fox, *Gaussian 09, Revision A.02*, Gaussian, Inc., Wallingford, CT, USA, 2009.

44 R. Gresser, A. Hoyer, M. Hummert, H. Hartmann, K. Leo and M. Riede, 3483, *Dalton Trans.*, 2011, **40**, 3476; N. G. Connelly and W. E. Geigerm, *Chem. Rev.*, 1996, **96**, 877–910.

45 Highly doped n^+-Si wafers were used as substrates and a layer of 300 nm of silicon dioxide (SiO_2: grown by thermal oxidation) was used as a gate dielectric layer. Cr(10 nm)/Au(20 nm) was successively evaporated and photolithographically delineated to obtain source and drain electrodes. Interdigitated structures of the drain–source contacts (channel length (L): 25 or 5 μm, channel wide (W): 294 or 38 mm) were used.

46 LED: C503C-WAN-CCADB231 is provided by Cree, Inc. Typical luminous intensity of the LED is defined as 35 000 mcd at current value of 20 mA (minimum 25 000 mcd to maximum 45 000 mcd). In our experiments, the I_{LED} was set at 12.9 mA (up to 3.0 V applied). This can be estimated to be 0.68 times the typical luminous intensity of 35 000 mcd. The relationship between light intensity and other I_{LED} values is summarized in Fig. S11 (ESI†).

47 Mobilities (μ) were calculated in the saturation regime by using the relationship: $\mu_{sat} = (2I_{DS}L)/[WC_{ox}(V_G - V_{th})^2]$, where C_{ox} is the oxide capacitance. The V_{th} values can be estimated as the intercept of the linear section of the plot of $(I_{DS})^{1/2}$ *vs.* V_G.

48 Conductivities were calculated using the following relationship: $S/m = (L/WF) \times (I_{DS}/V_{DS})$, where F is film thickness. The film thickness is approximately 60 nm (Fig. S13, ESI).

49 T. Mori, A. Kobayashi, Y. Sasaki, H. Kobayashi, G. Saito and H. Inokuchi, *Bull. Chem. Soc. Jpn.*, 1984, **57**, 627–633.